

On the Abundance of Potassium in Metal-Poor Stars

Yoichi TAKEDA

Komazawa University, Komazawa, Setagaya, Tokyo 154-8525

takedayi@cc.nao.ac.jp

Gang ZHAO, Yu-Qin CHEN, and Hong-Mei QIU

National Astronomical Observatories, Chinese Academy of Sciences, Beijing 100012, P. R. China

and

Masahide TAKADA-HIDAI

Liberal Arts Education Center, Tokai University, Hiratsuka, Kanagawa 259-1292

(Received 2001 October 8; accepted 2002 February 20)

Abstract

Based on extensive statistical-equilibrium calculations, we performed a non-LTE analysis of the K I 7699 equivalent-width data of metal-deficient stars for the purpose of clarifying the behavior of the photospheric potassium abundance in disk/halo stars. While the resulting non-LTE abundance corrections turned out to be considerably large, amounting to 0.2–0.7 dex, their effect on the [K/Fe] vs. [Fe/H] relation is not very important, since these corrections do not show any significant metallicity dependence. Hence, we again confirmed the results of previous LTE studies, that [K/Fe] shows a gradual systematic increase toward a lowered metallicity up to $[K/Fe] \sim 0.3\text{--}0.5$ at $[Fe/H] \sim -1$ to -2 , such as in the case of α elements.

Key words: Galaxy: evolution — line: formation — stars: abundances — stars: atmospheres — stars: late-type

1. Introduction

Among the elements for which abundances can be spectroscopically determined in metal-poor stars to investigate the chemical history of our Galaxy, our current knowledge about potassium (K; $Z = 19$) is still very insufficient in the sense that considerable ambiguities are involved in both the theoretical galactic chemical evolution calculation regarding [K/Fe] and the observational aspect of K abundance determination.

Theoretical investigations on the chemical evolution of this alkali element still suffer rather large uncertainties. Based on Woosely and Weaver's (1995; hereinafter WW95) yields and Salpeter's (1955) Initial Mass Function (IMF), Timmes et al. (1995) suggested a decreasing trend of [K/Fe] with a lowering of [Fe/H] (i.e., negative [K/Fe] in the metal-poor regime). Even when the Fe yield of WW95 is reduced by a factor of 2 (which they suggested to be more reasonable), their [K/Fe] barely exceeds ~ 0 (cf. their figure 24). Unfortunately, such a tendency apparently contradicted the observational implication of supersolar [K/Fe] (just like α elements) in metal-poor stars (see the next paragraph). This situation was improved by a recent calculation of Goswami and Prantzos (2000),

who also used the metallicity-dependent yields of WW95 (with a reduction of Fe yield by a factor of 2), but the more realistic IMF of Kroupa et al. (1993) (along with their own halo model). Their resulting $[K/Fe]$ shows a mildly supersolar behavior of $[K/Fe] \sim +0.2$ (cf. figure 7 therein). However, even this still appears to be somewhat insufficient to account for the observed $[K/Fe]$, amounting up to $\sim +0.5$. If a more satisfactory consistency is to be further pursued, the K yield itself would have to be adequately adjusted, such as was done by Samland (1998), who used a K yield about twice as large as that of WW95 (along with a Fe yield of about half that of WW95) and Salpeter IMF, by which he could reproduce the tendency that $[K/Fe]$ gradually increases from ~ 0 (at $[Fe/H] \sim 0$) to $\sim +0.3$ (at $[Fe/H] \sim -1$) and maintains a nearly constant value of $[K/Fe] \sim +0.3$ at $-3 \lesssim [Fe/H] \lesssim -1$, being nearly similar to the observed trend (see below). We should bear in mind, however, that such empirical adjustments of the yields are involved in his calculation.

Let us then turn our attention to the observational side. As far as we know, there have been only two studies which attempted to investigate the potassium abundance of metal-deficient stars. Gratton and Sneden (1987a,b) were the first to determine the K abundances of disk/halo stars (dwarfs as well as giants) in the metallicity range of $-2.5 \lesssim [Fe/H] \lesssim +0.3$ by using the K I resonance doublet lines at 7664.87 Å and 7698.98 Å. Meanwhile, Chen et al. (2000) recently carried out an extensive investigation on the chemical composition of mildly metal-poor ($-1 \lesssim [Fe/H] \lesssim 0$) F–G disk dwarfs, and determined the abundance of K, being included as one of their target elements, by using the K I 7698.98 Å line. Interestingly, both of these two studies suggested a gradually increasing trend of $[K/Fe]$ with a lowering of the metallicity at $-1 \lesssim [Fe/H] \lesssim 0$ (though with a rather large diversity), as has usually been referred to by theoreticians in comparing their computed predictions with observations. However, these authors do not appear to be sufficiently confident about the results which they obtained, since various difficulties are involved in the spectroscopic determination of the K abundance.

It should be kept in mind that only the resonance doublet lines (K I 7665 and 7699) are practically available, since other subordinate lines (cf. Lambert, Warner 1968) are either too weak to be measurable in metal-poor stars, or are located in an unfavorable wavelength region ($\lambda \sim 1.2 \mu\text{m}$). Unfortunately, however, these resonance lines are not necessarily suitable for an abundance determination for the following reasons:

- They occasionally suffer appreciable contaminations of the telluric O₂ lines; this blending effect is often more serious for the K I 7665 line.
- Since they are sufficiently strong to be saturated, the abundance is appreciably affected by the choice of the microturbulent velocity, which may be uncertain owing to its possible depth-dependence.
- Similarly, due to their considerable strengths, the abundances are more or less influenced by the adopted damping constant, which is not well established.
- They are considered to suffer a significantly large non-LTE effect; for example, according to the calculation of Takeda et al. (1996), the non-LTE abundance correction for the Sun (G2 V) and Procyon (F5 III–IV) amounts to -0.4 dex and -0.7 dex, respectively.
- In addition, because of its low ionization potential, only a very small number of potassium atoms remain neutral (i.e., almost all are in the once-ionization stage), which means that the abundance is sensitive to the atmospheric model (e.g., a choice of T_{eff}).

Presumably because of these difficulties, stellar spectroscopists may have somewhat hesitated to struggle with the potassium abundance of metal-poor stars.

Considering this situation, we decided to visit this problem by performing a non-LTE analysis on the observational K I 7699 data of the two studies mentioned above, while aiming to elucidate the behavior of [K/Fe] in metal-deficient stars, in order to provide theoreticians with observational information on the galactic [K/Fe] vs. [Fe/H] relation, while extensive non-LTE calculations were carried out on model atmospheres over a wide range of parameters for this purpose. This was the primary motivation of the present study.

We describe the adopted observational data in section 2. A description of our non-LTE calculations is presented in section 3. Our abundance determination procedure is explained in section 4, followed by section 5, where the possible uncertainties involved in the resulting abundances are estimated. The results are finally summarized in section 6.

2. Observational Data

The main observational data which we adopted were, similarly to those used by Chen et al. (2000), the spectra of 21 mildly metal-poor F–G stars observed by the Coudé Echelle Spectrograph attached to the 2.16 m telescope at Beijing Astronomical Observatory. See Chen et al. (2000) for more details. Figure 1 shows the 7692–7722 Å portion of these spectra, the S/N ratio of which was estimated to be 150–300. Based on these spectra, the equivalent width of the K I 7699 line was remeasured by one of us (Y.T.), either by Gaussian fitting or direct integration, depending on the situation. A comparison of such measured equivalent widths (which are given in table 1) with those used by Chen et al. (2000) (though the equivalent-width data for individual stars are not published therein) is shown in figure 2, from which we can see that the agreement is quite satisfactory. Namely, the observational data of these 22 stars (BAO samples) adopted in this study are essentially the same as those used by Chen et al. (2000).

Then, we also invoked the K I 7699 equivalent-width data of 24 metal-poor dwarfs and giants published by Gratton and Sneden (1987b), which were used in Gratton and Sneden’s (1987a) analysis. (Their K I 7665 data were not used, since we tried to make a consistent comparison.) These data are also presented in table 1. Note that two stars, HD 34411 and HD 142373, are common to both samples.

Regarding the K I 7699 equivalent width for the Sun, which was used as the reference standard, we measured it on the solar flux spectrum published by Kurucz et al. (1984; cf. figure 1) by the direct-integration method, and obtained 169.9 mÅ, which we eventually adopted. This value was further checked on the Moon spectrum observed at BAO. Although the K I 7699 line profile on this BAO spectrum shows a slight asymmetry in the damping wing (cf. figure 1), and is thus comparatively less suitable for an accurate measurement, we confirmed that the resulting equivalent-width (Moon) is in fairly good agreement (to within a few mÅ) with our adopted value.

3. Statistical Equilibrium Calculations

The procedures of our non-LTE calculations for neutral potassium were the same as that described in Takeda et al. (1996), which should be consulted for details. We only mention here that the H I collision rates in rate equations were drastically suppressed to a negligible level by multiplying the classical rates by a factor of 10^{-3} ($h = -3$) according to the consequence of Takeda et al. (1996).

Since we planned to make our calculations applicable to stars from near-solar metallicity

(population I) down to very low metallicity (extreme population II) at late-F through early-K spectral types in various evolutionary stages (i.e., dwarfs, subgiants, giants, and supergiants), we carried out non-LTE calculations on an extensive grid of one hundred ($5 \times 5 \times 4$) model atmospheres resulting from combinations of five T_{eff} values (4500, 5000, 5500, 6000, 6500 K), five $\log g$ values (1.0, 2.0, 3.0, 4.0, 5.0), and four metallicities (represented by $[\text{Fe}/\text{H}]$) (0.0, -1.0, -2.0, -3.0). As for the stellar model atmospheres, we adopted Kurucz's (1993) ATLAS9 models corresponding to a microturbulent velocity (ξ) of 2 km s⁻¹.

Regarding the potassium abundance used as an input value in non-LTE calculations, we assumed $\log \epsilon_{\text{K}}^{\text{input}} = 5.12 + [\text{Fe}/\text{H}] + [\text{K}/\text{Fe}]$, where $[\text{K}/\text{Fe}] = 0.0$ for the solar metallicity models ($[\text{Fe}/\text{H}] = 0$) and $[\text{K}/\text{Fe}] = +0.5$ for the other metal-deficient models ($[\text{Fe}/\text{H}] = -1, -2$, and -3). Namely, the solar potassium abundance of 5.12 (Anders, Grevesse 1989; Grevesse, Sauval 2000) was adopted for the normal-metal models, while a metallicity-scaled potassium abundance plus 0.5 dex (allowing for the characteristics suggested from two observational studies so far; cf. section 1) was assigned to the metal-poor models. The microturbulent velocity (appearing in the line-opacity calculations along with the abundance) was assumed to be 2 km s⁻¹, to make it consistent with the model atmosphere.

In figure 3 are shown the $S_{\text{L}}(\tau)/B(\tau)$ (the ratio of the line source function to the Planck function, and nearly equal to $\simeq b_2/b_1$, where b_1 and b_2 are the non-LTE departure coefficients for the lower and upper levels of the K I 7699 transition, respectively) and $l_0^{\text{NLTE}}(\tau)/l_0^{\text{LTE}}(\tau)$ (the NLTE-to-LTE line-center opacity ratio, and nearly equal to $\simeq b_1$) for a representative set of model atmospheres. We can read the following characteristics from this figure:

- In almost all cases, the inequality relations of $S_{\text{L}}/B < 1$ (dilution of line source function) and $l_0^{\text{NLTE}}/l_0^{\text{LTE}} > 1$ (enhanced line-opacity) hold in the important line-forming region, which means that the non-LTE effect always acts in the direction of strengthening the K I 7699 line.
- There is a tendency that the non-LTE effect is enhanced with a lowering of the gravity, as expected.
- The departure from LTE appears to be larger for higher T_{eff} in the high-metallicity (1×) case, while this trend becomes ambiguous, or even inverse, in the low-metallicity case.
- Toward a lower metallicity, the extent of the non-LTE departure tends to decrease, but the departure appears to penetrate deeper in the atmosphere, which makes the situation rather complex.
- For a very strong damping-dominated case (i.e., lowest T_{eff} and highest metallicity), the departure from LTE shifts toward the upper atmosphere and the non-LTE effect becomes comparatively insignificant.

Based on the results of these calculations, we computed an extensive grid of the theoretical equivalent-widths and the corresponding non-LTE corrections of the K I 7699 line for each of the model atmospheres, which are presented in the Appendix.

4. Abundance Analysis

Regarding T_{eff} (effective temperature), $\log g$ (surface gravity), $[\text{Fe}/\text{H}]$ (model metallicity), and ξ (microturbulence), we simply adopted the same values as those presented in Chen et al. (2000) and Gratton and Sneden (1987a), where we assigned the $[\text{Fe}/\text{H}]$ values spectroscopically determined by them to the model-metallicity (i.e., not the same model-metallicity as adopted by them). The

solar ξ value was assumed to be 1.4 km s^{-1} (Y.-Q. Chen, unpublished), which was determined in the same way using the Fe I lines as was done by Chen et al. (2000). Although this is appreciably larger than that derived from Takeda et al.'s (1996) solar flux spectrum analysis of K I 7699 as the best value (0.8 km s^{-1} ; cf. subsubsection 5.1.1 therein), we preferred to adopt this Fe I-based ξ value in order to maintain the consistency of the analysis, considering the differential nature of [K/Fe] in which we are most interested. These atmospheric parameters are given in table 1.

As for the model atmospheres, Kurucz's (1993) grid of ATLAS9 models was used as in the case of non-LTE calculations, based on which the model of each star was obtained by a three-dimensional interpolation with respect to T_{eff} , $\log g$, and [Fe/H]. Similarly, the depth-dependent departure coefficients (b) of neutral-potassium levels computed for the grid of models (cf. section 3) were interpolated in terms of T_{eff} , $\log g$, and [Fe/H], in order to evaluate the $S_{\text{L}}(\tau)/B(\tau)$ and $l_0^{\text{NLTE}}(\tau)/l_0^{\text{LTE}}(\tau)$ ratios for each star.

We used the WIDTH9 program written by R. L. Kurucz for determining the potassium abundance from the K I 7699 equivalent width, which had been modified to incorporate the non-LTE departure in the line source function as well as in the line opacity. The adopted line data for the K I line at 7698.98 \AA are essentially the same as those used or determined by Takeda et al. (1996): $\log gf = -0.17$ (Wiese et al. 1969; NIST database) for the oscillator strength, $\Gamma_{\text{rad}} = 0.38 \times 10^8 \text{ s}^{-1}$ (Wiese et al. 1969; NIST database) for the radiation damping constant, and $\Delta \log C_6 = +1.0$ (Takeda et al. 1996) for the correction applied to the classical Unsöld's (1955) formula for the van der Waals effect damping constant (i.e., $\log \Gamma_6 = \log \Gamma_6^{\text{classical}} + 0.4 \Delta \log C_6$). Regarding the quadratic Stark effect damping (which is insignificant in late-type stars), we followed the default treatment of the WIDTH9 program (cf. Leushin, Topil'skaya 1987).

The resulting non-LTE abundance ($\log \epsilon_{\text{K}}^{\text{NLTE}}$) and the non-LTE abundance correction ($\equiv \log \epsilon_{\text{K}}^{\text{NLTE}} - \log \epsilon_{\text{K}}^{\text{LTE}}$) are presented in table 1, where the [K/Fe] values (K-to-Fe logarithmic abundance ratio relative to the Sun), defined as $\log \epsilon_{\text{K}}^{\text{NLTE}}(\text{star}) - \log \epsilon_{\text{K}}^{\text{NLTE}}(\text{Sun}) - [\text{Fe}/\text{H}]$, are also given.

Although our reference solar potassium abundance (4.85) is apparently smaller than the standard solar value of 5.12 (Anders, Grevesse 1989; Grevesse, Sauval 2000), this is due to our adopted ξ value of 1.4 km s^{-1} , mentioned above, as well as the use of the ATLAS9 solar model. If we use Holweger and Müller's (1974) model with a ξ value of $0.8\text{--}1.0 \text{ km s}^{-1}$, we would obtain a value of ~ 5.1 (cf. table 4 in Takeda et al. 1996).

5. Error Estimations

Some discussion may be due concerning the uncertainty in the resulting abundances. Thanks to the simple ionization nature of potassium atoms, where almost all of the potassium atoms are in the ground state of the first-ionized stage, and only a small fraction of them remain neutral, the number population of the ground level of the neutral atoms (n_1 , which is proportional to the line opacity, l , of the K I 7699 line) is expressed as $n_1 \propto \epsilon \theta^{3/2} n_e 10^{\chi_1 \theta}$ according to Saha's equation (ϵ is the potassium abundance, $\theta \equiv 5040/T$, χ_1 is the ionization potential of 4.34 eV, and n_e is the electron density). Then, the dependence of the line-opacity (l) upon $\theta_{\text{eff}} (\equiv 5040/T_{\text{eff}})$ and g may be written as $l \propto \epsilon \theta_{\text{eff}}^{3/2} g^{1/3} 10^{\chi_1 \theta_{\text{eff}}}$ where we put $\theta \sim \theta_{\text{eff}}$ and used the approximation that the atmospheric density (pressure) roughly scales as $\propto g^{1/3}$ (see, e.g., Gray 1992). Consequently, the abundance (ϵ) resulting from a given equivalent width is dependent upon θ_{eff} and g as $\epsilon \propto \theta_{\text{eff}}^{-3/2} 10^{-\chi_1 \theta_{\text{eff}}} g^{-1/3}$, which suggests

that changes of $\Delta T_{\text{eff}} = \pm 200$ K and $\Delta \log g = \pm 0.3$ produce variations of $\sim \pm 0.15$ and $\sim \pm 0.10$ (for the case of $T_{\text{eff}} = 6000$ K and $\log g = 4$ atmosphere), respectively. In table 1 are given the actually computed changes corresponding to these perturbations of T_{eff} and $\log g$, which are to an order of magnitude consistent with such a rough analytical estimation.¹

Another important factor of uncertainty is the microturbulent velocity. Although most of the ξ values adopted in this study have been reasonably established by Chen et al. (2000) and Gratton and Sneden (1987a) in a conventional way using the Fe I lines, there is no guarantee that such values are safely applicable to an analysis of the strong K I line, because an adequate value of this parameter differs from line to line, reflecting the possible depth-dependence of the atmospheric velocity field (cf. subsubsection 5.1.1 in Takeda et al. 1996). As a matter of fact, by comparing the adopted values of the microturbulence with the estimated values based on the empirical formula proposed by Edvardsson et al. (1993), which is applicable to dwarf stars, we found that Chen et al.'s (2000) ξ values for BAO samples are slightly larger [by $0.2 (\pm 0.2)$ km s⁻¹ on the average], while the ξ values adopted by Gratton and Sneden (1987a) for their high-gravity samples turn out to be somewhat smaller [by $-0.3 (\pm 0.5)$ km s⁻¹ on the average], compared to the formula values. Hence, it should be kept in mind that rather significant ambiguities are involved in the ξ values given in table 1. We obtained abundance variations corresponding to changes of ± 0.5 km s⁻¹ (tentatively assigned uncertainty), which amount to ~ 0.1 – 0.2 dex, as given in table 1.

We also evaluated the errors caused by ambiguities in the damping parameter, for which van der Waals effect damping (Γ_6) is most important in the present case. Since Takeda et al. (1996) concluded the most adequate $\Delta \log C_6$ value to be $+1.0 (\pm 0.4)$ (cf. subsubsection 5.1.3 therein), we computed the abundance variations corresponding to this uncertainty range, which are also presented in table 1. As can be seen from this table, they are typically $\lesssim 0.1$ dex and may be comparatively less significant.

Based on what has been described above, it would be reasonable to state that the potassium abundances we have obtained are inevitably subject to rather large ambiguities amounting to $\lesssim 0.2$ – 0.3 dex.

6. Discussion and Conclusion

The finally resulting [K/Fe] vs. [Fe/H] relation and $\Delta \log \epsilon$ (non-LTE correction) vs. [Fe/H] relation are shown in figures 4a and b, respectively.

In figure 4a, we can observe a trend that [K/Fe] gradually increases with a decrease in [Fe/H] for disk stars, from [K/Fe] ~ 0 (at [Fe/H] ~ 0) to [K/Fe] ~ 0.3 – 0.4 (at [Fe/H] ~ -1), and appears to be nearly flat (or showing a weak further increase?) at the halo star region ([Fe/H] $\lesssim -1$), which is similar to that of the α -process elements (e.g., Mg, Si, Ca, etc.) as is well known. Especially, a systematic tight correlation exhibited by BAO sample stars (filled circles) is quite impressive. We also note that no clear difference exists between giants and dwarfs, as recognized from Gratton and Sneden's (1987) samples (open symbols). This tendency is almost the same as the results which Gratton and Sneden (1987a) and Chen et al. (2000) obtained in their LTE analyses.

As can be seen from figure 4b, the potassium abundances suffer considerably large non-LTE

¹ That the extent of Δ_g^\pm is somewhat smaller than the analytical prediction may presumably be due to the effect of the continuum opacity which is also affected by a density variation through the population of H⁺ ions.

corrections amounting to 0.2–0.7 dex (~ 0.5 dex on the average), which suggests that LTE is by no means an adequate assumption for determining the potassium abundance from the strong resonance K I line. However, since the extents of these corrections do not show any appreciable [Fe/H]-dependence (except for the high-metallicity region of $[\text{Fe}/\text{H}] \gtrsim 0$), the resultant non-LTE [K/Fe] vs. [Fe/H] diagram turned out to be almost similar to the LTE case. This is the reason why our new non-LTE analysis has confirmed the previous results.

In summary, the conclusions are as follows, based on our non-LTE analysis of the K I 7699 line data of metal-poor stars:

- (1) This resonance K I line suffers a considerable non-LTE effect (0.2–0.7 dex in terms of the abundance correction) which should be taken into consideration. However, since the non-LTE correction does not show any strong systematic [Fe/H]-dependence, its influence is not very significant as far as [K/Fe] (differential abundance ratio relative to the Sun) is concerned.
- (2) We confirmed the previously reported results that [K/Fe] gradually increases with a decrease in [Fe/H] for disk stars by ~ 0.3 –0.4 dex over the range $-1 \lesssim [\text{K}/\text{Fe}] \lesssim 0$, and appears to be nearly flat (or slightly increasing further) at the halo star region of $[\text{K}/\text{Fe}] \lesssim -1$.
- (3) Current standard galactic chemical evolution calculations, such as that of Timmes et al. (1995) using WW95 yields (as they are) and Salpeter IMF, do not appear to satisfactorily reproduce this behavior of supersolar [K/Fe] in metal-poor stars. In order to bring the theory into consistency with the observation, one has to invoke (i) some adjustment of the yields [e.g., reducing the WW95 Fe yield by a factor of 2 as suggested by Timmes et al. (1995), increasing the WW95 K yield as was done by Samland et al. (1998)] and/or (ii) the use of more realistic IMF [e.g., that of Kroupa et al. (1993) adopted by Goswami and Prantzos (2000)].

We thank Dr. N. Prantzos and an anonymous referee for pointing out our misunderstanding in the first version of this paper concerning the galactic chemical evolution calculations for K. This work was done within the framework of the China–Japan collaboration project, “Galactic Chemical Evolution through Spectroscopic Analyses of Metal-Deficient Stars” supported by the Japan Society for the Promotion of Science (JSPS) and the National Science Foundation of China (NSFC).

Appendix 1. Non-LTE Corrections for a Grid of Models

For the reader’s convenience, we present here an extensive grid of non-LTE abundance corrections for model atmospheres of various parameters, which have been computed as follows.

For an appropriately assigned potassium abundance (A^a) and microturbulence (ξ^a), we first calculated the non-LTE equivalent width (W^{NLTE}) of the line by using the computed non-LTE departure coefficients (b) for each model atmosphere. Next, the LTE (A^L) and NLTE (A^N) abundances were computed from this W^{NLTE} while regarding it as if being a given observed equivalent width. We can then obtain the non-LTE abundance correction, Δ , which is defined in terms of these two abundances as $\Delta \equiv A^N - A^L$.

Strictly speaking, the departure coefficients [$b(\tau)$] for a model atmosphere correspond to the potassium abundance and the microturbulence of $\log \epsilon_K^{\text{input}}$ and 2 km s^{-1} adopted in the non-LTE calculations (cf. section 3). Nevertheless, considering the fact that the departure coefficients (i.e., ratios of NLTE to LTE number populations) are (unlike the population itself) not much sensitive

to small changes in atmospheric parameters,² we also applied such computed b values to evaluating Δ for slightly different A^a and ξ^a from those fiducial values assumed in the statistical equilibrium calculations.

Hence, we evaluated Δ for three A^a values ($\log \epsilon_K^{\text{input}}$ and ± 0.3 dex perturbation) as well as three ξ values (2 km s^{-1} and $\pm 1 \text{ km s}^{-1}$ perturbation) for a model atmosphere using the same departure coefficients. We used the WIDTH9 program with the same line data as in section 4 for calculating the equivalent width for a given abundance, or inversely evaluating the abundance for an assigned equivalent width. We give only the $\xi = 2 \text{ km s}^{-1}$ results for the K I 7699 line in table 2. The complete data tables ($\xi = 1, 2$, and 3 km s^{-1}), which have been computed not only for the K I 7699 line but also for the K I 7665 line ($\lambda = 7664.87\text{\AA}$, $\log gf = +0.13$), along with a small Fortran program for using/interpolating these tables, are electronically available from the following anonymous ftp site:

ftp://www.ioa.s.u-tokyo.ac.jp/Users/takeda/potassium_nonlte/
(IP address: 133.11.160.242).

References

- [] Anders, E., & Grevesse, N. 1989, *Geochim. Cosmochim. Acta*, 53, 197
- [] Chen, Y. Q., Nissen, P. E., Zhao, G., Zhang, H. W., & Benoni, T. 2000, *A&AS*, 141, 491
- [] Edvardsson, B., Andersen, J., Gustafsson, B., Lambert, D. L., Nissen, P. E., & Tomkin, J. 1993, *A&A*, 275, 101
- [] Goswami, A., & Prantzos, N. 2000, *A&A*, 359, 191
- [] Gratton, R. G., & Sneden, C. 1987a, *A&A*, 178, 179
- [] Gratton, R. G., & Sneden, C. 1987b, *A&AS*, 68, 193
- [] Gray, D. F. 1992, *The Observation and Analysis of Stellar Photospheres*, 2nd ed. (Cambridge: Cambridge University Press), ch.9
- [] Grevesse, N., & Sauval, A. J. 2000, *Origin of Elements in the Solar System*, ed. O. Manuel (New York: Plenum Publishers), 261
- [] Holweger, H., & Müller, E. A. 1974, *Sol. Phys.*, 39, 19
- [] Kurucz, R. L. 1993, Kurucz CD-ROM, No. 13 (Harvard-Smithsonian Center for Astrophysics)
- [] Lambert, D., & Warner, B. 1968, *MNRAS*, 138, 181
- [] Leushin, V. V., & Topil'skaya, G. P. 1987, *Astrophysics*, 25, 415
- [] Kroupa, P., Tout, C. A., & Gilmore, G. 1993, *MNRAS*, 262, 545
- [] Kurucz, R. L., Furenlid, I., Brault, J., & Testerman, L. 1984, *Solar Flux Atlas from 296 to 1300 nm* (Sunspot, New Mexico: National Solar Observatory)
- [] Salpeter, E. E. 1955, *ApJ*, 121, 161
- [] Samland, M. 1998, *ApJ*, 496, 155
- [] Takeda, Y., Kato, K., Watanabe, Y., & Sadakane, K. 1996, *PASJ*, 48, 511
- [] Timmes, F. X., Woosley, S. E., & Weaver, T. A. 1995, *ApJS*, 98, 617
- [] Unsöld, A. 1955, *Physik der Sternatmosphären*, 2nd ed. (Berlin: Springer), 333
- [] Wiese, W. L., Smith, M. W., & Miles, B. M. 1969, *Atomic Transition Probabilities Vol.II — Sodium Through Calcium*, NSRDS-NBS22 (Washington, DC: US Government Printing Office)

² For example, a test analysis on the t60g40m1 model (with $W_{\lambda}^{7699} = 158 \text{ m\AA}$ and $\xi = 2 \text{ km s}^{-1}$) showed that the use of two kinds of b values computed with two different $\log \epsilon_K^{\text{input}}$ corresponding to $[\text{K}/\text{Fe}] = 0.0$ and $+0.5$ leads to almost the same non-LTE abundances (i.e., the differences amounting to only ~ 0.03 dex).

[] Woosely, S. E., & Weaver, T. A. 1995, ApJS, 101, 181 (WW95)

Table 1. Adopted Data of the Program Stars and the Results of the Analysis.

Star (HD)	T_{eff} (K)	$\log g$ (cm s^{-2})	[Fe/H]	ξ (km s^{-1})	W_{λ}	$\Delta \log \epsilon \log \epsilon$	[K/Fe]	Δ_{ξ}^{-}	Δ_{ξ}^{+}	Δ_{C}^{-}	Δ_{C}^{+}	Δ_{T}^{-}	Δ_{T}^{+}	Δ_{g}^{-}	Δ_{g}^{+}	
[Analysis of the Solar Flux Equivalent Width]																
Sun	5780	4.44	0.00	1.4	169.9	-0.38	4.85	0.00	+0.12	-0.13	+0.07	-0.08	-0.16	+0.15	+0.08	-0.09
[Analysis of the Remeasured Data of BAO Spectra]																
34411	5773	4.02	+0.01	1.7	162.6	-0.48	4.76	-0.10	+0.16	-0.15	+0.03	-0.05	-0.16	+0.15	+0.05	-0.05
19373	5867	4.01	+0.03	1.8	165.9	-0.51	4.82	-0.06	+0.17	-0.15	+0.03	-0.04	-0.16	+0.15	+0.04	-0.05
10307	5776	4.13	-0.05	1.8	167.5	-0.48	4.74	-0.06	+0.16	-0.14	+0.04	-0.05	-0.16	+0.15	+0.05	-0.06
68146	6227	4.16	-0.09	2.1	144.9	-0.57	4.73	-0.03	+0.13	-0.11	+0.01	-0.03	-0.14	+0.14	+0.03	-0.03
22484	5915	4.03	-0.13	2.0	163.2	-0.57	4.72	0.00	+0.15	-0.13	+0.02	-0.04	-0.16	+0.15	+0.04	-0.04
39587	5805	4.29	-0.18	2.2	168.6	-0.49	4.60	-0.07	+0.14	-0.11	+0.04	-0.04	-0.16	+0.15	+0.04	-0.05
142860	6227	4.18	-0.22	2.2	132.8	-0.56	4.57	-0.06	+0.12	-0.08	+0.02	-0.02	-0.14	+0.13	+0.02	-0.03
69897	6243	4.28	-0.28	2.0	136.9	-0.58	4.64	+0.07	+0.12	-0.09	+0.03	-0.02	-0.14	+0.13	+0.03	-0.03
55575	5802	4.36	-0.36	1.6	141.7	-0.48	4.47	-0.02	+0.12	-0.11	+0.04	-0.05	-0.16	+0.16	+0.05	-0.06
142373	5920	4.27	-0.39	1.5	137.9	-0.54	4.54	+0.08	+0.12	-0.11	+0.04	-0.05	-0.16	+0.15	+0.05	-0.06
101676	6102	4.09	-0.47	2.0	131.6	-0.61	4.49	+0.11	+0.12	-0.09	+0.02	-0.02	-0.14	+0.14	+0.03	-0.03
76349	6004	4.21	-0.49	2.1	132.0	-0.56	4.40	+0.04	+0.10	-0.08	+0.02	-0.03	-0.15	+0.14	+0.03	-0.03
118244	6234	4.13	-0.55	2.3	126.0	-0.60	4.46	+0.16	+0.10	-0.07	+0.01	-0.02	-0.13	+0.12	+0.02	-0.02
109303	5905	4.10	-0.61	1.7	122.2	-0.58	4.32	+0.08	+0.11	-0.09	+0.03	-0.03	-0.15	+0.14	+0.03	-0.04
41640	6004	4.37	-0.62	2.0	114.8	-0.51	4.25	+0.02	+0.08	-0.07	+0.02	-0.03	-0.15	+0.14	+0.03	-0.03
62301	5837	4.23	-0.67	1.7	126.9	-0.54	4.30	+0.12	+0.11	-0.09	+0.04	-0.04	-0.16	+0.15	+0.04	-0.05
49732	6260	4.15	-0.70	1.9	104.5	-0.58	4.34	+0.19	+0.09	-0.07	+0.01	-0.02	-0.13	+0.12	+0.02	-0.02
106516	6135	4.34	-0.71	1.5	112.6	-0.57	4.39	+0.25	+0.10	-0.08	+0.03	-0.03	-0.14	+0.13	+0.04	-0.04
208906	5929	4.39	-0.73	1.5	112.5	-0.52	4.25	+0.13	+0.08	-0.08	+0.03	-0.04	-0.15	+0.14	+0.04	-0.05
60319	5867	4.24	-0.85	1.6	117.2	-0.55	4.24	+0.24	+0.09	-0.08	+0.03	-0.04	-0.16	+0.14	+0.04	-0.05
201891	5827	4.43	-1.04	1.6	101.4	-0.47	4.04	+0.23	+0.07	-0.06	+0.03	-0.04	-0.16	+0.14	+0.04	-0.04
[Reanalysis of Gratton and Sneden's (1987b) Data]																
4614	5670	4.30	-0.33	1.0	122.0	-0.43	4.35	-0.17	+0.09	-0.11	+0.05	-0.06	-0.17	+0.16	+0.06	-0.07
6582	5250	4.50	-0.75	1.0	145.0	-0.34	4.07	-0.03	+0.06	-0.08	+0.09	-0.09	-0.21	+0.19	+0.09	-0.10
6755	5260	3.00	-1.67	2.7	93.9	-0.41	3.53	+0.35	+0.05	-0.04	+0.00	-0.01	-0.18	+0.15	+0.02	-0.02
33256	6140	3.91	-0.58	1.2	121.0	-0.69	4.61	+0.34	+0.12	-0.13	+0.02	-0.04	-0.14	+0.13	+0.04	-0.05
34411	5840	4.10	+0.16	1.0	156.0	-0.42	4.99	-0.02	+0.12	-0.17	+0.06	-0.08	-0.16	+0.15	+0.07	-0.08
58551	6000	4.50	-0.78	1.0	112.0	-0.52	4.35	+0.28	+0.07	-0.08	+0.05	-0.06	-0.15	+0.14	+0.06	-0.07
59984	5840	4.01	-0.93	1.0	121.4	-0.60	4.41	+0.49	+0.09	-0.11	+0.04	-0.06	-0.16	+0.15	+0.06	-0.07
63077	5660	4.11	-0.94	0.8	136.3	-0.51	4.43	+0.52	+0.07	-0.10	+0.08	-0.08	-0.18	+0.17	+0.09	-0.09
76932	5630	3.88	-1.01	0.8	102.3	-0.55	4.10	+0.26	+0.07	-0.09	+0.05	-0.05	-0.17	+0.16	+0.06	-0.06
102870	6080	4.11	+0.06	1.2	155.6	-0.51	5.04	+0.13	+0.15	-0.16	+0.05	-0.06	-0.15	+0.14	+0.06	-0.07
103095	5000	4.50	-1.15	1.0	118.0	-0.30	3.55	-0.15	+0.04	-0.06	+0.07	-0.08	-0.23	+0.21	+0.08	-0.08
107328	4560	2.70	-0.31	1.7	225.7	-0.27	4.50	-0.04	+0.24	-0.26	+0.06	-0.07	-0.27	+0.25	+0.07	-0.08
122563	4640	1.30	-2.38	2.0	37.1	-0.26	2.55	+0.08	+0.03	-0.02	+0.00	-0.00	-0.21	+0.16	+0.04	-0.04
122956	4660	1.75	-1.93	1.7	120.8	-0.60	3.49	+0.57	+0.19	-0.13	+0.01	-0.01	-0.26	+0.22	+0.07	-0.06
128620	5750	4.38	+0.11	1.2	174.1	-0.35	4.96	0.00	+0.11	-0.14	+0.08	-0.08	-0.16	+0.16	+0.09	-0.10
128621	5250	4.50	+0.08	1.0	250.1	-0.18	5.03	+0.10	+0.06	-0.08	+0.13	-0.13	-0.22	+0.20	+0.14	-0.14
134169	5750	4.50	-1.02	1.0	106.0	-0.46	4.09	+0.26	+0.06	-0.06	-0.05	-0.17	+0.16	+0.06	-0.07	
140573	4600	2.75	+0.36	1.5	254.9	-0.13	5.07	-0.14	+0.20	-0.28	+0.08	-0.09	-0.26	+0.25	+0.09	-0.10
142373	5760	3.90	-0.36	1.0	121.0	-0.55	4.45	-0.04	+0.11	-0.13	+0.04	-0.05	-0.16	+0.16	+0.05	-0.06
161096	4600	2.70	+0.24	1.4	259.8	-0.12	5.13	+0.04	+0.17	-0.25	+0.09	-0.10	-0.27	+0.26	+0.10	-0.11
165195	4500	1.20	-2.21	2.0	115.0	-0.49	3.27	+0.63	+0.16	-0.11	+0.01	+0.00	-0.29	+0.21	+0.08	-0.08
175305	5160	3.00	-1.53	2.0	110.0	-0.52	3.68	+0.36	+0.11	-0.08	+0.02	-0.01	-0.20	+0.17	+0.03	-0.03
221170	4500	1.30	-1.96	1.4	134.0	-0.63	3.62	+0.73	+0.27	-0.21	+0.01	-0.02	-0.30	+0.25	+0.09	-0.09
224930	5250	4.50	-0.84	1.0	177.0	-0.34	4.26	+0.25	+0.06	-0.07	+0.11	-0.10	-0.21	+0.20	+0.12	-0.12

Notes. The atmospheric parameters (T_{eff} , $\log g$, [Fe/H], and ξ) were taken from Chen et al. (2000), and Gratton and Sneden (1987a), for each data group, respectively. Given in the 7th and 8th columns are the non-LTE correction ($\equiv \log \epsilon_{\text{K}}^{\text{NLTE}} - \log \epsilon_{\text{K}}^{\text{LTE}}$) and the non-LTE abundance ($\log \epsilon_{\text{K}}^{\text{NLTE}}$; in the usual normalization of $\log \epsilon_{\text{H}} = 12.00$), respectively. The K to Fe logarithmic abundance ratio, [K/Fe], in the 9th column is defined as $\log \epsilon_{\text{K}}^{\text{NLTE}}(\text{star}) - \log \epsilon_{\text{K}}^{\text{NLTE}}(\text{Sun}) - [\text{Fe/H}]$. The abundance variations caused by changing the adopted parameters are given in 10th through 17th columns: changing the ξ value by -0.5 km s^{-1} (Δ_{ξ}^{-}) and $+0.5 \text{ km s}^{-1}$ (Δ_{ξ}^{+}), changing the $\Delta \log C_6$ value (with respect to the fiducial value of +1.0) by -0.4 (Δ_{C}^{-}) and $+0.4$ (Δ_{C}^{+}), changing the T_{eff} value by -200 K (Δ_{T}^{-}) and $+200 \text{ K}$ (Δ_{T}^{+}), and changing the $\log g$ value by -0.3 (Δ_{g}^{-}) and $+0.3$ (Δ_{g}^{+}).

Table 2. NLTE abundance correction for K I 7698.98 ($\xi = 2 \text{ km s}^{-1}$).

Code	$A_1^a (W_1^{\text{LTE}})$	W_1^{NLTE}	A_1^N	A_1^L	Δ_1	$A_2^a (W_2^{\text{LTE}})$	W_2^{NLTE}	A_2^N	A_2^L	Δ_2	$A_3^a (W_3^{\text{LTE}})$	W_3^{NLTE}	A_3^N	A_3^L	Δ_3
t65g50m0	4.820 (97.72)	138.04 4.819 5.236	-0.417	5.120 (125.89)	177.83 5.120 5.562	-0.442	5.420 (158.49)	223.87 5.425 5.847	-0.422						
t65g40m0	4.820 (87.10)	131.83 4.812 5.439	-0.627	5.120 (107.15)	165.96 5.130 5.840	-0.710	5.420 (131.83)	199.53 5.439 6.149	-0.710						
t65g30m0	4.820 (81.28)	131.83 4.828 5.590	-0.762	5.120 (102.33)	162.18 5.130 6.043	-0.913	5.420 (120.23)	190.55 5.427 6.409	-0.982						
t65g20m0	4.820 (83.18)	134.90 4.830 5.651	-0.821	5.120 (102.33)	162.18 5.105 6.094	-0.989	5.420 (120.23)	190.55 5.413 6.519	-1.106						
t65g10m0	4.820 (75.86)	125.89 4.816 5.613	-0.797	5.120 (95.50)	154.88 5.107 6.096	-0.989	5.420 (114.82)	181.97 5.398 6.537	-1.139						
t60g50m0	4.820 (138.04)	181.97 4.827 5.171	-0.344	5.120 (173.78)	229.09 5.117 5.449	-0.332	5.420 (223.87)	288.40 5.410 5.708	-0.298						
t60g40m0	4.820 (117.49)	165.96 4.827 5.390	-0.563	5.120 (141.25)	199.53 5.117 5.685	-0.568	5.420 (169.82)	239.88 5.437 5.953	-0.516						
t60g30m0	4.820 (107.15)	162.18 4.836 5.597	-0.761	5.120 (128.82)	190.55 5.120 5.935	-0.815	5.420 (147.91)	218.78 5.410 6.209	-0.799						
t60g20m0	4.820 (102.33)	158.49 4.826 5.681	-0.855	5.120 (123.03)	186.21 5.118 6.092	-0.974	5.420 (141.25)	213.80 5.428 6.447	-1.019						
t60g10m0	4.820 (102.33)	158.49 4.823 5.701	-0.878	5.120 (123.03)	186.21 5.120 6.136	-1.016	5.420 (141.25)	213.80 5.439 6.531	-1.092						
t55g50m0	4.820 (199.53)	245.47 4.832 5.074	-0.242	5.120 (257.04)	309.03 5.110 5.328	-0.218	5.420 (338.84)	407.38 5.429 5.618	-0.189						
t55g40m0	4.820 (154.88)	204.17 4.832 5.254	-0.422	5.120 (186.21)	245.47 5.135 5.520	-0.385	5.420 (229.09)	295.12 5.432 5.763	-0.331						
t55g30m0	4.820 (141.25)	190.55 4.816 5.435	-0.619	5.120 (162.18)	223.87 5.145 5.749	-0.604	5.420 (190.55)	251.19 5.400 5.955	-0.555						
t55g20m0	4.820 (134.90)	186.21 4.807 5.560	-0.753	5.120 (154.88)	213.80 5.111 5.900	-0.789	5.420 (177.83)	239.88 5.404 6.168	-0.764						
t55g10m0	4.820 (128.82)	186.21 4.844 5.675	-0.831	5.120 (147.91)	208.93 5.100 5.997	-0.897	5.420 (169.82)	234.42 5.406 6.315	-0.909						
t50g50m0	4.820 (323.59)	371.54 4.819 4.965	-0.146	5.120 (436.52)	489.78 5.109 5.238	-0.129	5.420 (588.84)	676.08 5.425 5.541	-0.116						
t50g40m0	4.820 (218.78)	263.03 4.823 5.070	-0.247	5.120 (275.42)	323.59 5.127 5.332	-0.205	5.420 (346.74)	407.38 5.429 5.596	-0.167						
t50g30m0	4.820 (186.21)	229.09 4.826 5.217	-0.391	5.120 (218.78)	263.03 5.119 5.467	-0.348	5.420 (257.04)	302.00 5.401 5.684	-0.283						
t50g20m0	4.820 (177.83)	218.78 4.815 5.326	-0.511	5.120 (199.53)	245.47 5.111 5.598	-0.487	5.420 (229.09)	275.42 5.421 5.848	-0.427						
t50g10m0	4.820 (173.78)	218.78 4.850 5.422	-0.572	5.120 (194.98)	239.88 5.105 5.668	-0.563	5.420 (218.78)	263.03 5.384 5.914	-0.530						
t45g50m0	4.820 (630.96)	707.95 4.828 4.923	-0.095	5.120 (870.96)	954.99 5.121 5.206	-0.085	5.420 (202.26)	288.25 5.411 5.483	-0.072						
t45g40m0	4.820 (380.19)	416.87 4.829 4.934	-0.105	5.120 (501.19)	537.03 5.112 5.196	-0.084	5.420 (676.08)	724.44 5.412 5.485	-0.073						
t45g30m0	4.820 (269.15)	295.12 4.811 4.961	-0.150	5.120 (323.59)	354.81 5.121 5.234	-0.113	5.420 (407.38)	436.52 5.411 5.492	-0.081						
t45g20m0	4.820 (239.88)	263.03 4.825 5.014	-0.189	5.120 (275.42)	295.12 5.117 5.268	-0.151	5.420 (316.23)	338.84 5.432 5.540	-0.108						
t45g10m0	4.820 (239.88)	251.19 4.791 4.969	-0.178	5.120 (263.03)	281.84 5.145 5.303	-0.158	5.420 (295.12)	309.03 5.423 5.553	-0.130						
t65g50m1	4.320 (57.54)	93.33 4.314 4.746	-0.432	4.620 (83.18)	131.83 4.619 5.136	-0.517	4.920 (109.65)	173.78 4.920 5.463	-0.543						
t65g40m1	4.320 (52.48)	91.20 4.328 4.906	-0.578	4.620 (72.44)	123.03 4.626 5.372	-0.746	4.920 (91.20)	154.88 4.922 5.757	-0.835						
t65g30m1	4.320 (48.98)	87.10 4.312 4.932	-0.620	4.620 (67.61)	117.49 4.608 5.464	-0.856	4.920 (87.10)	147.91 4.914 5.966	-1.052						
t65g20m1	4.320 (51.29)	91.20 4.314 5.000	-0.686	4.620 (69.18)	123.03 4.628 5.586	-0.958	4.920 (87.10)	151.36 4.920 6.095	-1.175						
t65g10m1	4.320 (45.71)	85.11 4.325 4.970	-0.645	4.620 (64.57)	114.82 4.619 5.509	-0.890	4.920 (83.18)	144.54 4.925 6.058	-1.133						
t60g50m1	4.320 (87.10)	138.04 4.317 4.764	-0.447	4.620 (120.23)	186.21 4.613 5.085	-0.472	4.920 (158.49)	245.47 4.916 5.374	-0.458						
t60g40m1	4.320 (74.13)	123.03 4.310 4.951	-0.641	4.620 (97.72)	158.49 4.613 5.322	-0.709	4.920 (120.23)	194.98 4.908 5.607	-0.699						
t60g30m1	4.320 (70.79)	120.23 4.331 5.128	-0.797	4.620 (89.13)	151.36 4.632 5.585	-0.953	4.920 (107.15)	181.97 4.940 5.937	-0.997						
t60g20m1	4.320 (67.61)	117.49 4.332 5.172	-0.840	4.620 (85.11)	147.91 4.634 5.701	-1.067	4.920 (102.33)	173.78 4.908 6.106	-1.198						
t60g10m1	4.320 (69.18)	117.49 4.311 5.165	-0.854	4.620 (87.10)	147.91 4.618 5.714	-1.096	4.920 (104.71)	177.83 4.941 6.220	-1.279						
t55g50m1	4.320 (141.25)	208.93 4.323 4.700	-0.377	4.620 (194.98)	275.42 4.610 4.977	-0.367	4.920 (257.04)	371.54 4.925 5.267	-0.342						
t55g40m1	4.320 (109.65)	169.82 4.335 4.895	-0.560	4.620 (138.04)	208.93 4.611 5.158	-0.547	4.920 (173.78)	263.03 4.932 5.428	-0.496						
t55g30m1	4.320 (95.50)	154.88 4.335 5.117	-0.782	4.620 (117.49)	186.21 4.627 5.432	-0.805	4.920 (138.04)	218.78 4.922 5.681	-0.759						
t55g20m1	4.320 (91.20)	147.91 4.318 5.248	-0.930	4.620 (109.65)	177.83 4.626 5.663	-1.037	4.920 (128.82)	204.17 4.910 5.957	-1.047						
t55g10m1	4.320 (87.10)	144.54 4.319 5.292	-0.973	4.620 (104.71)	173.78 4.628 5.778	-1.150	4.920 (123.03)	199.53 4.920 6.151	-1.231						
t50g50m1	4.320 (251.19)	338.84 4.330 4.598	-0.268	4.620 (346.74)	457.09 4.627 4.879	-0.252	4.920 (478.63)	616.60 4.913 5.153	-0.240						
t50g40m1	4.320 (169.82)	234.42 4.331 4.714	-0.383	4.620 (218.78)	295.12 4.629 4.970	-0.341	4.920 (281.84)	371.54 4.911 5.212	-0.301						
t50g30m1	4.320 (138.04)	194.98 4.313 4.887	-0.574	4.620 (165.96)	234.42 4.633 5.157	-0.524	4.920 (199.53)	275.42 4.918 5.372	-0.454						
t50g20m1	4.320 (125.89)	186.21 4.342 5.108	-0.766	4.620 (147.91)	213.80 4.628 5.378	-0.750	4.920 (169.82)	245.47 4.947 5.624	-0.677						
t50g10m1	4.320 (120.23)	177.83 4.317 5.193	-0.876	4.620 (138.04)	204.17 4.612 5.530	-0.918	4.920 (158.49)	229.09 4.902 5.798	-0.896						
t45g50m1	4.320 (446.68)	588.84 4.326 4.565	-0.239	4.620 (630.96)	812.83 4.629 4.859	-0.230	4.920 (870.96)	96.48 4.916 5.132	-0.216						
t45g40m1	4.320 (302.00)	371.54 4.312 4.528	-0.216	4.620 (407.38)	489.78 4.614 4.799	-0.185	4.920 (562.34)	660.69 4.912 5.081	-0.169						
t45g30m1	4.320 (213.80)	263.03 4.322 4.621	-0.299	4.620 (263.03)	316.23 4.608 4.853	-0.245	4.920 (338.84)	398.11 4.923 5.114	-0.191						
t45g20m1	4.320 (186.21)	229.09 4.312 4.728	-0.416	4.620 (213.80)	263.03 4.622 4.975	-0.353	4.920 (257.04)	302.00 4.917 5.193	-0.276						
t45g10m1	4.320 (177.83)	218.78 4.304 4.788	-0.484	4.620 (204.17)	245.47 4.611 5.059	-0.448	4.920 (229.09)	275.42 4.936 5.318	-0.382						

Table 2. (Continued.)

Code	$A_1^a (W_1^{\text{LTE}})$	W_1^{NLTE}	A_1^N	A_1^L	Δ_1	$A_2^a (W_2^{\text{LTE}})$	W_2^{NLTE}	A_2^N	A_2^L	Δ_2	$A_3^a (W_3^{\text{LTE}})$	W_3^{NLTE}	A_3^N	A_3^L	Δ_3
t65g50m2	3.320 (10.23)	16.98 3.321 3.569	-0.248	3.620 (18.62)	30.90 3.622 3.885	-0.263	3.920 (33.11)	52.48 3.921 4.217	-0.296						
t65g40m2	3.320 (9.77)	16.98 3.316 3.593	-0.277	3.620 (17.78)	30.90 3.625 3.925	-0.300	3.920 (30.90)	50.12 3.913 4.256	-0.343						
t65g30m2	3.320 (8.91)	16.22 3.316 3.614	-0.298	3.620 (16.60)	29.51 3.625 3.944	-0.319	3.920 (28.18)	48.98 3.927 4.293	-0.366						
t65g20m2	3.320 (9.55)	17.78 3.325 3.629	-0.304	3.620 (17.38)	31.62 3.626 3.958	-0.332	3.920 (29.51)	51.29 3.920 4.313	-0.393						
t65g10m2	3.320 (8.13)	15.14 3.319 3.627	-0.308	3.620 (14.79)	27.54 3.624 3.955	-0.331	3.920 (25.70)	45.71 3.919 4.297	-0.378						
t60g50m2	3.320 (17.38)	30.20 3.326 3.600	-0.274	3.620 (31.62)	52.48 3.622 3.920	-0.298	3.920 (52.48)	85.11 3.926 4.266	-0.340						
t60g40m2	3.320 (17.38)	30.20 3.320 3.619	-0.299	3.620 (30.20)	51.29 3.624 3.966	-0.342	3.920 (47.86)	77.62 3.915 4.336	-0.421						
t60g30m2	3.320 (16.60)	29.51 3.318 3.634	-0.316	3.620 (28.84)	48.98 3.614 3.977	-0.363	3.920 (45.71)	74.13 3.912 4.376	-0.464						
t60g20m2	3.320 (15.49)	28.18 3.317 3.646	-0.329	3.620 (26.92)	47.86 3.624 4.001	-0.377	3.920 (42.66)	72.44 3.923 4.398	-0.475						
t60g10m2	3.320 (16.60)	29.51 3.316 3.639	-0.323	3.620 (28.84)	48.98 3.613 3.992	-0.379	3.920 (44.67)	74.13 3.916 4.413	-0.497						
t55g50m2	3.320 (31.62)	56.23 3.324 3.628	-0.304	3.620 (54.95)	93.33 3.620 3.954	-0.334	3.920 (89.13)	144.54 3.923 4.296	-0.373						
t55g40m2	3.320 (30.90)	52.48 3.314 3.655	-0.341	3.620 (50.12)	83.18 3.622 4.032	-0.410	3.920 (74.13)	117.49 3.914 4.409	-0.495						
t55g30m2	3.320 (30.20)	51.29 3.317 3.676	-0.359	3.620 (47.86)	79.43 3.628 4.094	-0.466	3.920 (67.61)	109.65 3.933 4.556	-0.623						
t55g20m2	3.320 (28.84)	50.12 3.320 3.694	-0.374	3.620 (45.71)	75.86 3.617 4.097	-0.480	3.920 (64.57)	104.71 3.923 4.592	-0.669						
t55g10m2	3.320 (26.92)	47.86 3.315 3.696	-0.381	3.620 (43.65)	74.13 3.625 4.110	-0.485	3.920 (61.66)	102.33 3.929 4.596	-0.667						
t50g50m2	3.320 (74.13)	117.49 3.316 3.609	-0.293	3.620 (120.23)	186.21 3.625 3.947	-0.322	3.920 (181.97)	269.15 3.915 4.256	-0.341						
t50g40m2	3.320 (63.10)	100.00 3.325 3.688	-0.363	3.620 (93.33)	141.25 3.611 4.033	-0.422	3.920 (125.89)	190.55 3.909 4.356	-0.447						
t50g30m2	3.320 (54.95)	87.10 3.311 3.741	-0.430	3.620 (77.62)	120.23 3.610 4.161	-0.551	3.920 (100.00)	154.88 3.911 4.533	-0.622						
t50g20m2	3.320 (51.29)	83.18 3.326 3.805	-0.479	3.620 (70.79)	112.20 3.616 4.268	-0.652	3.920 (91.20)	141.25 3.909 4.716	-0.807						
t50g10m2	3.320 (47.86)	79.43 3.320 3.809	-0.489	3.620 (67.61)	109.65 3.630 4.321	-0.691	3.920 (87.10)	138.04 3.931 4.825	-0.894						
t45g50m2	3.320 (151.36)	245.47 3.316 3.686	-0.370	3.620 (223.87)	354.81 3.615 3.998	-0.383	3.920 (323.59)	501.19 3.914 4.300	-0.386						
t45g40m2	3.320 (141.25)	194.98 3.330 3.645	-0.315	3.620 (190.55)	257.04 3.610 3.925	-0.315	3.920 (257.04)	346.74 3.922 4.220	-0.298						
t45g30m2	3.320 (109.65)	151.36 3.329 3.745	-0.416	3.620 (138.04)	190.55 3.620 4.049	-0.429	3.920 (173.78)	234.42 3.905 4.305	-0.400						
t45g20m2	3.320 (95.50)	134.90 3.326 3.842	-0.516	3.620 (117.49)	165.96 3.622 4.199	-0.577	3.920 (141.25)	199.53 3.940 4.505	-0.565						
t45g10m2	3.320 (87.10)	125.89 3.326 3.881	-0.555	3.620 (107.15)	154.88 3.626 4.282	-0.656	3.920 (128.82)	181.97 3.922 4.612	-0.690						
t65g50m3	2.320 (1.12)	1.82 2.323 2.532	-0.209	2.620 (2.24)	3.55 2.619 2.828	-0.209	2.920 (4.37)	6.92 2.916 3.126	-0.210						
t65g40m3	2.320 (1.10)	1.86 2.323 2.552	-0.229	2.620 (2.19)	3.63 2.619 2.849	-0.230	2.920 (4.27)	7.08 2.919 3.151	-0.232						
t65g30m3	2.320 (0.98)	1.74 2.318 2.570	-0.252	2.620 (1.95)	3.47 2.624 2.877	-0.253	2.920 (3.80)	6.76 2.921 3.175	-0.254						
t65g20m3	2.320 (0.81)	1.55 2.318 2.602	-0.284	2.620 (1.62)	3.09 2.615 2.891	-0.276	2.920 (3.31)	6.31 2.924 3.201	-0.277						
t65g10m3	2.320 (0.89)	1.62 2.318 2.585	-0.267	2.620 (1.74)	3.24 2.625 2.893	-0.268	2.920 (3.47)	6.31 2.925 3.196	-0.271						
t60g50m3	2.320 (2.04)	3.31 2.318 2.537	-0.219	2.620 (3.98)	6.46 2.621 2.842	-0.221	2.920 (7.76)	12.59 2.925 3.148	-0.223						
t60g40m3	2.320 (2.09)	3.39 2.319 2.541	-0.222	2.620 (4.07)	6.61 2.616 2.839	-0.223	2.920 (7.94)	12.88 2.925 3.153	-0.228						
t60g30m3	2.320 (1.95)	3.31 2.319 2.553	-0.234	2.620 (3.89)	6.46 2.617 2.850	-0.233	2.920 (7.59)	12.30 2.915 3.155	-0.240						
t60g20m3	2.320 (1.82)	3.16 2.316 2.565	-0.249	2.620 (3.55)	6.17 2.616 2.864	-0.248	2.920 (6.92)	12.02 2.924 3.178	-0.254						
t60g10m3	2.320 (1.66)	2.95 2.318 2.588	-0.270	2.620 (3.16)	5.62 2.615 2.882	-0.267	2.920 (6.17)	10.96 2.919 3.190	-0.271						
t55g50m3	2.320 (3.80)	6.46 2.322 2.558	-0.236	2.620 (7.41)	12.30 2.617 2.853	-0.236	2.920 (14.13)	23.44 2.917 3.158	-0.241						
t55g40m3	2.320 (3.98)	6.61 2.316 2.544	-0.228	2.620 (7.76)	12.88 2.622 2.854	-0.232	2.920 (14.79)	23.44 2.915 3.153	-0.238						
t55g30m3	2.320 (4.07)	6.61 2.320 2.542	-0.222	2.620 (7.76)	12.59 2.619 2.846	-0.227	2.920 (14.79)	22.91 2.917 3.152	-0.235						
t55g20m3	2.320 (3.98)	6.46 2.316 2.544	-0.228	2.620 (7.59)	12.30 2.618 2.850	-0.232	2.920 (14.13)	22.39 2.919 3.159	-0.240						
t55g10m3	2.320 (3.55)	6.17 2.325 2.565	-0.240	2.620 (6.92)	11.75 2.625 2.869	-0.244	2.920 (13.18)	21.38 2.922 3.175	-0.253						
t50g50m3	2.320 (7.08)	13.18 2.325 2.602	-0.277	2.620 (13.80)	25.12 2.619 2.899	-0.280	2.920 (26.30)	46.77 2.916 3.202	-0.286						
t50g40m3	2.320 (8.32)	14.45 2.325 2.575	-0.250	2.620 (15.85)	26.30 2.615 2.872	-0.257	2.920 (28.84)	46.77 2.918 3.187	-0.269						
t50g30m3	2.320 (8.71)	14.13 2.320 2.556	-0.236	2.620 (16.22)	25.70 2.619 2.864	-0.245	2.920 (28.18)	43.65 2.918 3.181	-0.263						
t50g20m3	2.320 (8.51)	13.49 2.322 2.546	-0.224	2.620 (15.49)	24.55 2.623 2.857	-0.234	2.920 (27.54)	41.69 2.925 3.180	-0.255						
t50g10m3	2.320 (8.13)	12.88 2.319 2.546	-0.227	2.620 (14.79)	23.44 2.621 2.859	-0.238	2.920 (26.30)	39.81 2.923 3.181	-0.258						
t45g50m3	2.320 (17.38)	34.67 2.323 2.642	-0.319	2.620 (33.11)	64.57 2.620 2.950	-0.330	2.920 (60.26)	120.23 2.921 3.263	-0.342						
t45g40m3	2.320 (18.62)	35.48 2.316 2.638	-0.322	2.620 (34.67)	63.10 2.620 2.957	-0.337	2.920 (58.88)	104.71 2.927 3.291	-0.364						
t45g30m3	2.320 (21.88)	34.67 2.324 2.566	-0.242	2.620 (38.02)	57.54 2.616 2.878	-0.262	2.920 (61.66)	89.13 2.919 3.223	-0.304						
t45g20m3	2.320 (19.95)	31.62 2.325 2.570	-0.245	2.620 (34.67)	51.29 2.616 2.884	-0.268	2.920 (53.70)	77.62 2.920 3.244	-0.324						
t45g10m3	2.320 (17.78)	28.18 2.323 2.572	-0.249	2.620 (30.90)	46.77 2.622 2.899	-0.277	2.920 (47.86)	70.79 2.924 3.260	-0.336						

Note. The case of $\xi = 2 \text{ km s}^{-1}$ calculation for the K I resonance line at 7698.98 Å. Code “taagbbmc” denotes the model with $T_{\text{eff}} = aa \times 100$, $\log g = bb/10$, and $[\text{Fe}/\text{H}]$ (metallicity) = $-c$. Calculations for each model were made three times corresponding to three assigned potassium abundances, A_i^a ($\equiv 5.12 + [\text{Fe}/\text{H}] + [\text{K}/\text{Fe}]_i$) ($i = 1, 2, 3$), where $([\text{K}/\text{Fe}]_1, [\text{K}/\text{Fe}]_2, [\text{K}/\text{Fe}]_3)$ are $(-0.3, 0.0, +0.3)$ for the solar metallicity models ($[\text{Fe}/\text{H}] = 0$) and $(+0.2, +0.5, +0.8)$ for all other metal-deficient models ($[\text{Fe}/\text{H}] = -1, -2, -3$). W_i^{LTE} and W_i^{NLTE} are the resulting theoretical LTE and NLTE equivalent widths (in mÅ) corresponding to the assigned A_i^a , respectively. Based on such calculated *non-LTE* equivalent width, W_i^{NLTE} , two kinds of potassium abundances were inversely computed for the cases of NLTE (A_i^N) and LTE (A_i^L), from which the non-LTE abundance correction was eventually evaluated as the difference of these two, Δ_i ($\equiv A_i^N - A_i^L$).

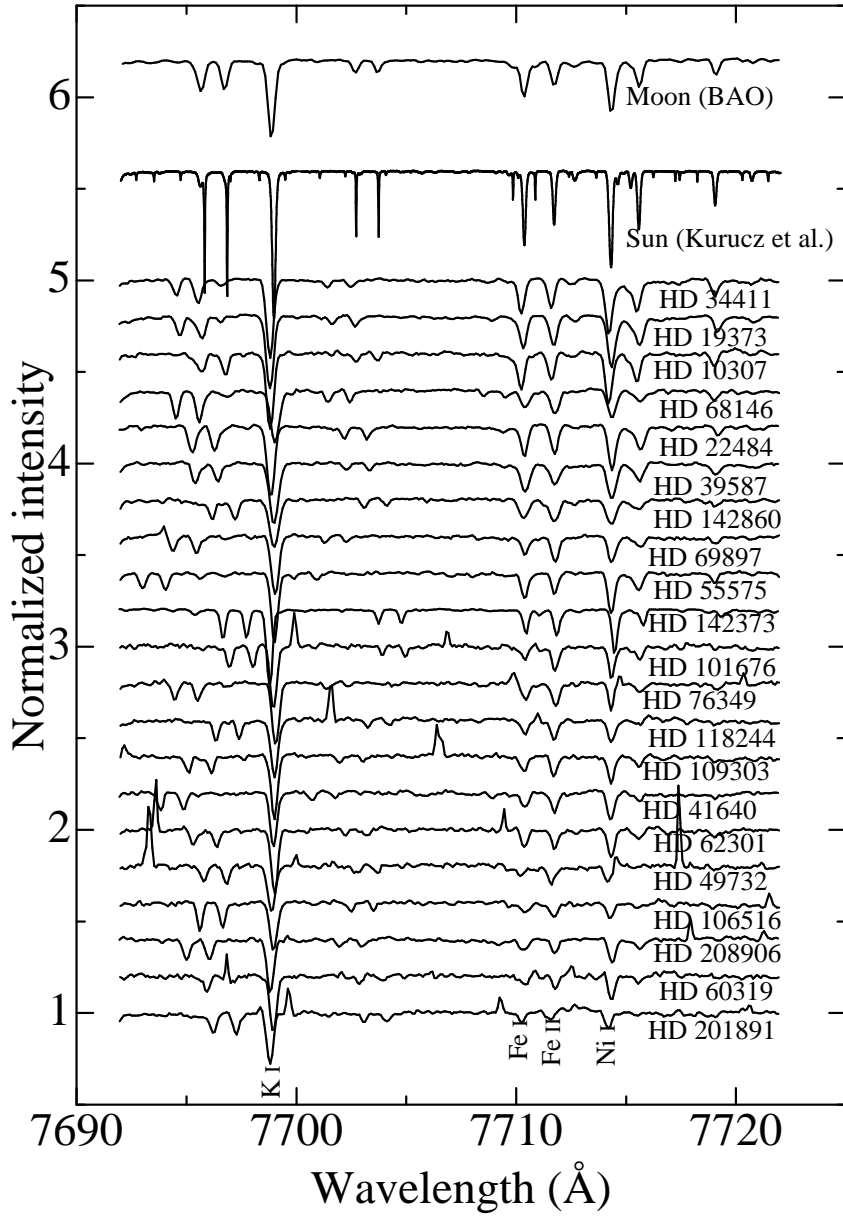


Fig. 1. BAO spectra of 21 mildly metal-poor F–G dwarfs (along with Kurucz et al.’s solar flux spectrum and the BAO Moon spectrum; cf. section 2) in the 7692–7722 Å region including the K I 7699 line. Each spectrum, normalized with respect to the continuum level, is vertically offset by 0.2 (except for 0.6 for the spectra of the Sun and the Moon) relative to the adjacent one.

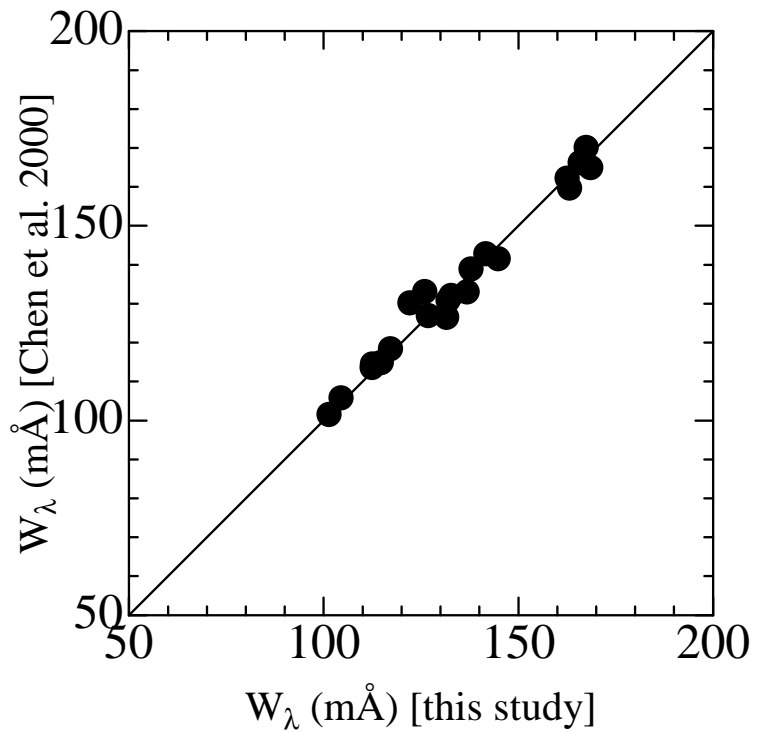


Fig. 2. Comparison of the K I 7699 equivalent widths of 21 stars used by Chen et al. (2000) with those newly remeasured by using the same spectra for this study.

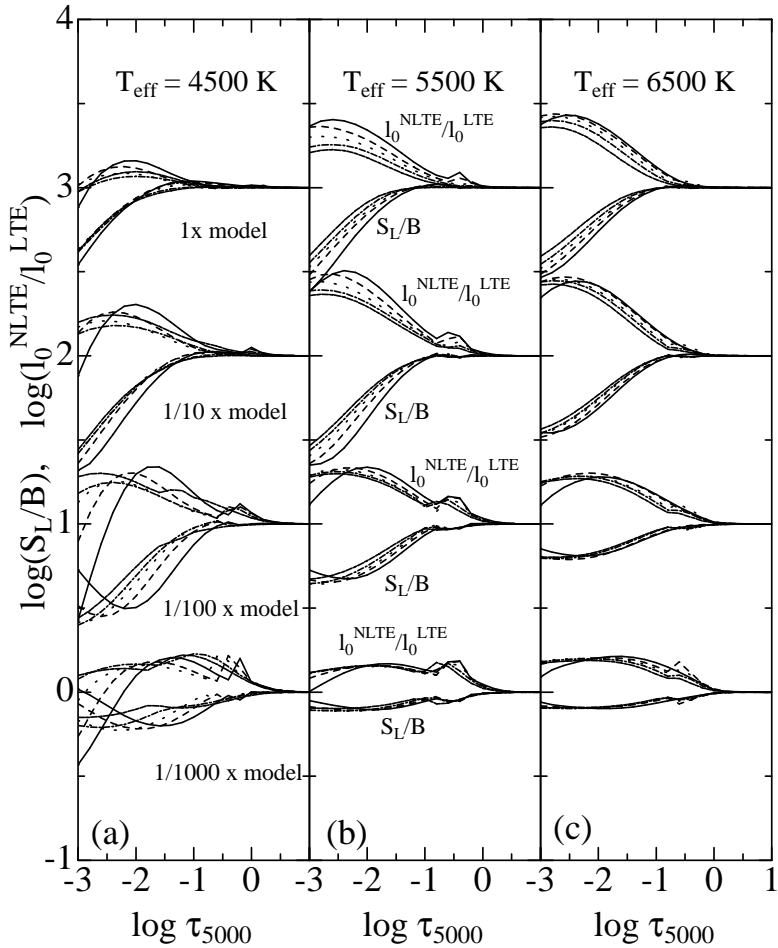


Fig. 3. Ratio of the line source function (S_L) to the local Planck function (B) and the NLTE-to-LTE line-center opacity ratio for the $4s\ ^2S-4p\ ^2P^o$ transition (corresponding to K I 7698.98 resonance line), which are shown as functions of the standard continuum optical depth at 5000 Å for models of $T_{\text{eff}} = 4500$ K, 5500 K, and 6500 K. The solid lines, dashed lines, dotted lines, dash-dotted lines, and dash-double-dotted lines correspond to the results for $\log g = 1.0, 2.0, 3.0, 4.0$, and 5.0, respectively. Note that the curves are vertically offset by an amount of 1.0 dex relative to those of the adjacent metallicity ones.

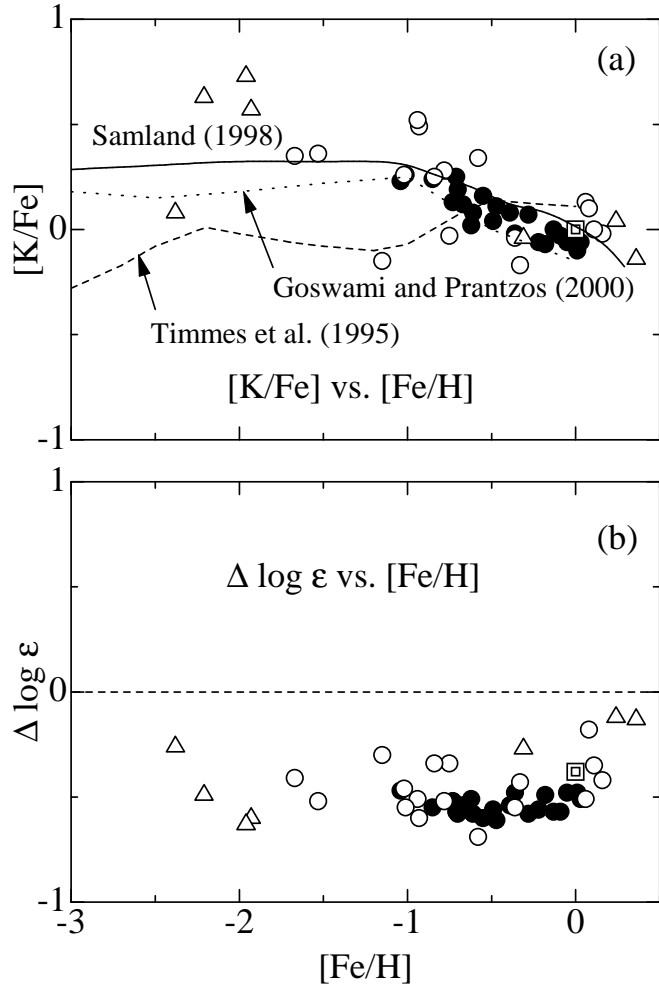


Fig. 4. (a) Resulting $[K/Fe]$ vs. $[Fe/H]$ relation constructed from the NLTE abundances of potassium for the program stars. Lines show the three kinds of theoretical predictions published so far (cf. section 1). Solid line — Samland (1998) (Salpeter IMF, adjusted K yield about twice as large as that of WW95, adjusted Fe yield about half as small as that of WW95), dashed line — Timmes et al. (1995) (Salpeter IMF, K yield of WW95, Fe yield of $0.5 \times$ WW95), dotted line — Goswami and Prantzos (2000) (their “Case B”, Kroupa et al.’s IMF, Fe yield of $0.5 \times$ WW95, K yield of WW95). The results for the BAO sample (22 mildly metal-poor F–G dwarfs) are shown by the filled circles, while those derived by reanalyzing Gratton and Sneden’s (1987b) equivalent widths for 24 metal-deficient stars are denoted by the open symbols (open circles — high-gravity stars with $\log g \geq 3.0$; open triangles — low-gravity stars with $\log g < 3.0$). The data for the Sun is indicated by the double square. (b) The NLTE correction for the K abundance for each star plotted as a function of $[Fe/H]$.